Spectroscopic Investigation of the Metal Ligation and Reactivity of the Ferrous Active Sites of Bleomycin and Bleomycin Derivatives

Kelly E. Loeb,[†] **Jeffrey M. Zaleski,**[†] **Cynthia D. Hess,**[‡] **Sidney M. Hecht,**[‡] **and Edward I. Solomon*,**[†]

Contribution from the Department of Chemistry, Stanford University, Stanford, California 94305-5080, and Departments of Chemistry and Biology, University of Virginia, Charlottesville, Virginia 22901

Received June 5, 1997

Abstract: The geometric and electronic structures of high-spin ferrous complexes of bleomycin (Fe^{II}BLM) and a series of systematically perturbed BLM derivatives have been investigated by optical absorption, circular dichroism (CD), and magnetic circular dichroism (MCD) spectroscopies. The active site of the unmodified drug complex is six-coordinate with the coordination sphere completed by at least five endogenous ligands including the pyrimidine, imidazole, deprotonated amide, and secondary and primary amine functionalities with either the 3-*O*-carbamoyl substituent of the mannose sugar or solvent bound at the sixth site. This weak sixth ligand is the exchangeable site of exogenous small molecule binding. Perturbing the carbamoyl substituent alters the coordination environment of the metal and decreases the azide binding affinities of the perturbed complexes. This is correlated with altered DNA cleaving capabilities. Additionally, altering the binding of the axial primary amine significantly affects the iron coordination sphere as evidenced by reduced π-back-bonding interactions specifically with the pyrimidine ligand. This pyrimidine π-back-bonding appears to play a key role in mediating the electron density localized on the ferrous center, which contributes to the unique oxygen chemistry and reactivity exhibited by Fe^{II}BLM relative to other non-heme iron sites. Oxygen binding to derivatives in which the β-aminoalanine fragment has been removed leads to a high-spin ferric complex and no observed DNA strand scission, in contrast to the long-lived low-spin activated BLM intermediate that precedes DNA degradation.

Introduction

Mononuclear non-heme iron active sites exist in a variety of systems which perform important biological functions requiring the binding and activation of dioxygen. These systems can be divided into classes based on the types of reactions they catalyze: dismutation (superoxide dismutase[1]), oxidation (*iso*penicillin N synthase[2]), extra- (catechol 2,3-dioxygenase) and intradiol (protocatechuate 3,4-dioxygenase) dioxygenation,[3,4] *cis*-dihydroxylation (phthalate dioxygenase[5]), pterin- (phenylalanine hydroxylase[6,7]) and α-ketoglutarate-dependent (clavaminate synthase[8]) hydroxylation, hydroperoxidation (soybean lipoxygenase[9]), and DNA cleavage (bleomycin[10−13]). Bleomycin (BLM)[14] is a glycopeptide antibiotic first isolated in 1966 as a

Cu^{II} complex from *Streptomyces verticillus*.[15,16] The drug Blenoxane is used most successfully in combination therapy for the treatment of a variety of carcinomas and lymphomas, apparently because of its ability to degrade duplex DNA[13,17] and possibly RNA[18] selectively. DNA degradation is oxygen- and metal ion-dependent[19−22] with the greatest enhancement and only in vivo activity observed for iron.[23−31] Oxygen binds to

† Stanford University.

‡ University of Virginia.

(1) Stoddard, B. L.; Howell, P. L.; Ringe, D.; Petsko, G. A. *Biochemistry* **1990**, *29*, 8885−8893.

(2) Baldwin, J. E.; Bradley, M. *Chem. Rev. (Washington, D.C.)* **1990**, *90*, 1079−1088.

(3) Que, L., Jr. *Iron Carriers and Iron Proteins*; Loehr, T. M., Ed.; VCH Publishers: Inc.: New York, 1989; Physical Bioinorganic Chemistry Series, Vol. 5, pp 467−524.

(4) Lipscomb, J. D.; Orville, A. M. *Metal Ions in Biological Systems*; Sigel, H., Sigel, A., Eds.; Marcel Dekker, Inc.: New York, 1992; Vol. 28, pp 243−298.

(5) Batie, C. J.; LaHaie, E.; Ballou, D. P. *J. Biol. Chem.* **1987**, *262*, 1510−1518.

(6) Shiman, R. *Folates and Pterins: Chemistry and Biochemistry of Pterins*; Blakley, R. L., Benkovic, S. J., Eds.; John Wiley & Sons: New York, 1985; Vol. 2, pp 179−249.

(7) Kappock, T. J.; Caradonna, J. P. *Chem. Rev.* **1996**, *96*, 2659−2756.

(8) Salowe, S. P.; Marsh, E. N.; Townsend, C. A. *Biochemistry* **1990**, *29*, 6499−6508.

(9) Samuelsson, B.; Dahlén, S.-E.; Lindgren, J. Å.; Rouzer, C. A.; Serhan, C. N. *Science* **1987**, *237*, 1171−1176.

(10) Hecht, S. M. *Acc. Chem. Res* **1986**, *19*, 383−391.

(11) Stubbe, J.; Kozarich, J. W. *Chem. Rev. (Washington, D.C.)* **1987**, *87*, 1107−1136.

(12) Natrajan, A.; Hecht, S. M. *Molecular Aspects of Anticancer Drug−DNA Interactions*; Neidle, S., Waring, M., Eds.; MacMillan: London, 1994; pp 197−242.

(13) Stubbe, J.; Kozarich, J. W.; Wu, W.; Vanderwall, D. E. *Acc. Chem. Res.* **1996**, *29*, 322−330.

(14) Abrreviations and terminology: bleomycin (BLM), *iso*-BLM (containing a 2-*O*-carbamoyl instead of a 3-*O*-carbamoyl group), decarbamoyl-BLM (lacking the 3-*O*-carbamoyl substituent), depyruvamide-BLM (DP-BLM, lacking the β-aminoalanine amide moiety), *N*-acetyl-BLM (having an *N*-acetylated primary amine within the β-aminoalanine amide moiety), *epi*-BLM (epimeric with BLM at C6), deamido-BLM (containing a β-aminoalanine moiety), peplomycin (PEPLM), circular dichroism (CD), electron paramagnetic resonance (EPR), magnetic circular dichroism (MCD), metal-to-ligand charge transfer (MLCT), near-infrared (NIR), nuclear magnetic resonance (NMR), variable-temperature variable-field (VTVH), zero-field-splitting (ZFS).

(15) Umezawa, H.; Surhara, Y.; Takita, T.; Maeda, K. *J. Antibiot.* **1966**, *19*, 210−219.

(16) Umezawa, H.; Maeda, K.; Takeuchi, T.; Oakami, Y. *J. Antibiot.* **1966**, *19*, 200−209.

(17) Hutchinson, F.; Povirk, L. F. *Bleomycin: Chemical, Biochemical, and Biological Aspects*; Hecht, S. M., Ed.; Springer-Verlag: New York, 1979; pp 255−266.

(18) Hecht, S. M. *Bioconjugate Chem.* **1994**, *5*, 513−526.

high-spin Fe^{II}BLM to produce oxygenated BLM (O$_2$-Fe^{II}BLM or O$_2^-$-Fe^{III}BLM)[32−34] and then accepts an additional electron to form activated BLM (O$_2^{2-}$-Fe^{III}BLM), which has been identified as a low-spin ferric-peroxide species.[28,33,35,36] This is the last detectable intermediate prior to DNA strand scission, and much effort is currently focused on developing a unified mechanism of DNA recognition and chemical specificity of cleavage.[13,37−44]

It remains unclear whether the peroxide species initiates DNA cleavage or undergoes hetero- or homolysis of the O−O bond forming a ferryl intermediate prior to, or concomitant with, reaction with substrate.[13,45−47] The similarity in mechanism to cytochrome P-450 and the ability to perform oxygen atom transfer reactions[48,49] have led researchers to postulate an oxo-ferryl-level BLM intermediate,[11,28] as has generally been considered to be present in heme chemistry.[50,51] Although BLM
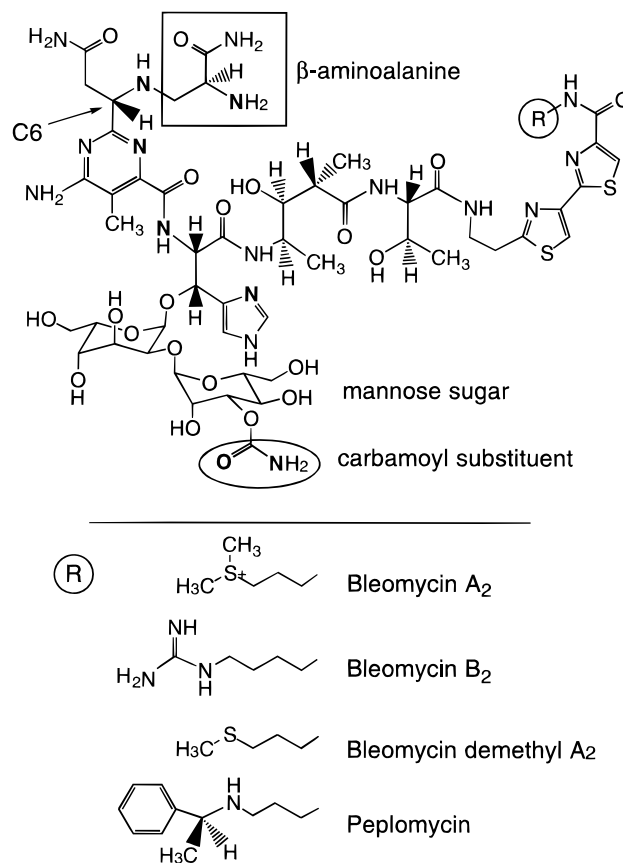

Figure 1. Bleomycin ligand framework. The bold atom labels indicate potential metal binding ligands.

is formally a non-heme iron system due to the absence of an extensive delocalized π-network, it deviates from this class of complexes due to the presence of moderately intense, low-energy metal-to-ligand charge transfer (MLCT) transitions which reflect strong Fe^{II}→pyrimidine back-bonding.[52] Relative to non-heme iron enzymes this π-back-bonding contributes to the unique chemistry and reactivity of Fe^{II}BLM; this includes its ability to reversibly bind CO[53] and to react with NO and other strong field ligands to form low-spin complexes.[54] For reaction with dioxygen, increased π-back-bonding relative to other non-heme sites results in reduced charge donation to the bound oxygen, stabilizing the initial O$_2^-$-Fe^{III}BLM intermediate from loss of superoxide and reaction with substrate and promoting the further reduction of O$_2^-$-Fe^{III}BLM to form activated BLM.[52] Thus, BLM can perhaps be viewed as bridging the chemistry between heme and non-heme iron systems.

No crystal structure exists for the ferrous complex of BLM and there is some controversy concerning the ligation of BLM to Fe^{II}. The ligand framework of several BLM congeners is shown in Figure 1 and differs only in the charge and chemical nature of the terminal amine substituent of the bithiazole. The potential metal-binding ligands are shown in bold for clarity. Present coordination descriptions based on correlations to a crystallographically defined Cu^{II} complex of a biosynthetic

(19) Ishida, R.; Takahashi, T. *Biochem. Biophys. Res. Commun.* **1975**, *66*, 1432−1438.

(20) Sausville, E. A.; Peisach, J.; Horwitz, S. B. *Biochemistry* **1978**, *17*, 2740−2746.

(21) Ehrenfeld, G. M.; Murugesan, N.; Hecht, S. M. *Inorg. Chem.* **1984**, *23*, 1496−1498.

(22) Ehrenfeld, G. M.; Shipley, J. B.; Heimbrook, D. C.; Sugiyama, H.; Long, E. C.; van Boom, J. H.; van der Marel, G. A.; Oppenheimer, N. J.; Hecht, S. M. *Biochemistry* **1987**, *26*, 931−942.

(23) Sausville, E. A.; Peisach, J.; Horwitz, S. B. *Biochem. Biophys. Res. Commun.* **1976**, *73*, 814−822.

(24) Lown, J. W.; Sim, S.-K. *Biochem. Biophys. Res. Commun.* **1977**, *77*, 1150−1157.

(25) Sausville, E. A.; Stein, R. W.; Peisach, J.; Horwitz, S. B. *Biochemistry* **1978**, *17*, 2746−2754.

(26) Burger, R. M.; Berkowitz, A. R.; Peisach, J.; Horwitz, S. B. *J. Biol. Chem.* **1980**, *255*, 11832−11838.

(27) Giloni, L.; Takeshita, M.; Johnson, F.; Iden, C.; Grollman, A. P. *J. Biol. Chem.* **1981**, *256*, 8608−8615.

(28) Burger, R. M.; Peisach, J.; Horwitz, S. B. *J. Biol. Chem.* **1981**, *256*, 11636−11644.

(29) McGall, G. H.; Rabow, L. E.; Ashley, G. W.; Wu, S. H.; Kozarich, J. W.; Stubbe, J. *J. Am. Chem. Soc.* **1992**, *114*, 4958−4967.

(30) Absalon, M. J.; Kozarich, J. W.; Stubbe, J. *Biochemistry* **1995**, *34*, 2065−2075.

(31) Absalon, M. J.; Wu, W.; Kozarich, J. W.; Stubbe, J. *Biochemistry* **1995**, *34*, 2076−2086.

(32) Albertini, J.-P.; Garnier-Suillerot, A.; Tosi, L. *Biochem. Biophys. Res. Commun.* **1982**, *104*, 557−563.

(33) Burger, R. M.; Kent, T. A.; Horwitz, S. B.; Münck, E.; Peisach, J. *J. Biol. Chem.* **1983**, *258*, 1559−1564.

(34) Fulmer, P.; Petering, D. H. *Biochemistry* **1994**, *33*, 5319−5327.

(35) Sam, J. W.; Tang, X.-J.; Peisach, J. *J. Am. Chem. Soc.* **1994**, *116*, 5250−5256.

(36) Westre, T. E.; Loeb, K. E.; Zaleski, J. M.; Hedman, B.; Hodgson, K. O.; Solomon, E. I. *J. Am. Chem. Soc.* **1995**, *117*, 1309−1313.

(37) Kane, S. A.; Hecht, S. M. *Prog. Nucleic Acid Res. Mol. Biol.* **1994**, *49*, 313−352.

(38) Povirk, L. F. *Mutat. Res.* **1996**, *355*, 71−89.

(39) Otvos, J. D.; Antholine, W. E.; Wehrli, S.; Petering, D. H. *Biochemistry* **1996**, *35*, 1458−1465.

(40) Mao, Q.; Fulmer, P.; Li, W.; DeRose, E. F.; Petering, D. H. *J. Biol. Chem.* **1996**, *271*, 6185−6191.

(41) Yang, Y.; Huang, L.; Pon, R. T.; Cheng, S.-F.; Chang, D.-K.; Lown, K. W. *Bioconjugate Chem.* **1996**, *7*, 670−679.

(42) Wu, W.; Vanderwall, D. E.; Turner, C. J.; Kozarich, J. W.; Stubbe, J. *J. Am. Chem. Soc.* **1996**, *118*, 1281−1294.

(43) Wu, W.; Vanderwall, D. E.; Lui, S. M.; Tang, X.-J.; Turner, C. J.; Kozarich, J. W.; Stubbe, J. *J. Am. Chem. Soc.* **1996**, *118*, 1268−1280.

(44) Fulmer, P.; Zhao, C.; Li, W.; DeRose, E.; Antholine, W. E.; Petering, D. H. *Biochemistry* **1997**, *36*, 4367−4374.

(45) Natrajan, A.; Hecht, S. M.; van der Marel, G. A.; van Boom, J. H. *J. Am. Chem. Soc.* **1990**, *112*, 4532−4538.

(46) Natrajan, A.; Hecht, S. M. *J. Org. Chem.* **1991**, *56*, 5239−5241.

(47) Burger, R. M.; Tian, G.; Drlica, K. *J. Am. Chem. Soc.* **1995**, *117*, 1167−1168.

(48) Murugesan, N.; Ehrenfeld, G.; Hecht, S. *J. Biol. Chem.* **1982**, *257*, 8600−8603.

(49) Murugesan, N.; Hecht, S. M. *J. Am. Chem. Soc.* **1985**, *107*, 493−500.

(50) Ortiz de Montellano, P. R. *Cytochrome P-450: Structure, Mechanism, and Biochemistry*; Plenum Press: New York, 1986.

(51) Selke, M.; Sisemore, M. F.; Ho, R. Y. N.; Wertz, D. L.; Valentine, J. S. *J. Mol. Catal. A: Chem.* **1997**, *117*, 71−82.

(52) Loeb, K. E.; Zaleski, J. M.; Westre, T. E.; Guajardo, R. J.; Mascharak, P. K.; Hedman, B.; Hodgson, K. O.; Solomon, E. I. *J. Am. Chem. Soc.* **1995**, *117*, 4545−4561.

(53) Oppenheimer, N. J.; Rodriguez, L. O.; Hecht, S. M. *Proc. Natl. Acad. Sci. U.S.A.* **1979**, *76*, 5616−5620.

(54) Sugiura, Y.; Suzuki, T.; Kawabe, H.; Tanaka, H.; Watanabe, K. *Biochim. Biophys. Acta* **1982**, *716*, 38−44.

precursor P-3A agree that the pyrimidine, imidazole, deprotonated amide, and secondary amine of the β-aminoalanine fragment are bound to the metal in a pseudo-square-planar arrangment.[55] There remains a question of axial ligation either by the primary amine of the β-aminoalanine fragment[43,52,56−61] and/or the carbamoyl substituent on the mannose sugar[53,62−65] (lacking in P-3A). Recent evidence from NMR studies on HOO-CoBLM is consistent with axial coordination by the primary amine;[42] however, most of the structural studies are complicated by the fact that they were performed on resting Zn- or Cd-BLMs, hydroperoxide-bound Co-BLM, or carbon monoxide-bound Fe-BLM and are not necessarily addressing the metal coordination environment in the active oxygen-binding ferrous form of the drug.

We have employed magnetic circular dichroism (MCD) spectroscopy[66] to study mononuclear non-heme ferrous systems which are often difficult to observe via other techniques.[52,67−72] MCD spectroscopy in the near-infrared (NIR) energy region allows one to directly observe ligand field d→d transitions. These excited-state d_σ-orbital energies are sensitive to the coordination number and geometry at the iron active site.[66] A six-coordinate, distorted octahedral iron center would exhibit two transitions centered around 10 000 cm^{-1} split by ∼2 000 cm^{-1}; a five-coordinate complex should have two transitions near 5 000 and 10 000 cm^{-1} with an excited-state splitting of ∼5000 cm^{-1}; and a four-coordinate tetrahedral complex should have $10Dq(T_d) = (-4/9)10Dq(O_h)$ giving rise to transitions in the 4000−7000 cm^{-1} region. In addition, variable-temperature variable-field (VTVH) MCD spectroscopy can be used to extract the ground-state sublevel splittings for these electron paramagnetic resonance (EPR) inactive non-Kramers ions which can then be related to the ground-state d_π-orbital energies. For a high-spin ferrous system with an $S = 2$ ground state the MCD saturation magnetization intensity exhibits "nesting" behavior (i.e., plots of MCD intensity monitored at given temperatures with variation in fields do not superimpose when plotted as a

function of $\beta H/2kT$) which can be explained in terms of zero-field-splitting (ZFS) of the $S = 2$ 5-fold degenerate ground state. For the more common $-D$ situation, this temperature and field dependence results from rhombic ZFS, by an amount δ, of the $M_s = \pm 2$ non-Kramers doublet electronic ground state. The value of δ is sensitive to the coordination number and geometry at the Fe active site: distorted octahedral six-coordinate sites will have $3 < \delta < 7$ cm^{-1} whereas five-coordinate sites will generally have smaller rhombic splittings of <4 cm^{-1} for square-pyramidal geometries and <3 cm^{-1} for trigonal-bipyramidal geometries. For the $+D$ case, similar behavior may result from a temperature- and field-dependent $\mathcal{B}$-term originating from an off-axis Zeeman interaction between the $M_s = 0$ ground state and one component of the $M_s = \pm 1$ excited state dependent on the polarization and orientation of the magnetic field.[66,73] VTVH MCD data can be used to distinguish the sign of D by iteratively fitting the field, temperature, and normalized MCD intensity as a function of δ and $g_{\parallel}$, and including the additional effects of linear $\mathcal{B}$-terms, z-polarization, and potential thermal population of excited states. The spin Hamiltonian parameters obtained through this analysis can be related to the axial and rhombic ligand field parameters Δ (the splitting of the d_{xy} and $d_{xz,yz}$ orbitals) and V (the splitting of the d_{xz} and d_{yz} orbitals) through the solution to the full $^5T_{2g}$ ligand field Hamiltonian.[66] Combining both the excited-state and ground-state analyses, an experimentally determined d-orbital energy level diagram is obtained which provides information about the geometric and electronic structure of the ferrous center and insight into oxygen binding and activation at these important mononuclear non-heme iron active sites.

This protocol applied to Fe^{II}BLM defined a six-coordinate, distorted octahedral geometry at the ferrous active site with a very small value of δ (2.4 cm^{-1}), which gives an unusually large $^5T_{2g}$ splitting.[52] In addition, short Fe−pyrimidine bond distances of 2.06 Å for Fe^{II}BLM and 2.00 Å for a model complex were identified by using X-ray absorption spectroscopy and correlated with the presence of low-energy Fe^{II} d_π→pyrimidine π^* MLCT transitions. These transitions were assigned by using resonance Raman profiles of the model complex in solution which showed enhancement of the pyrimidine ring vibrational modes by the absorption bands. Together, this information provided evidence of strong π-backbonding specifically with the pyrimidine ligand. On the basis of a comparison to a model complex which was five-coordinate in the solid state and six-coordinate in solution, solvent was proposed to coordinate trans to the primary amine with the pyrimidine, imidazole, deprotonated amide, and secondary amine functionalities bound in the equatorial plane. However, the model complex lacked both the sugar moiety and the bithiazole tail of the fully functionalized BLM ligand. We have now extended this methodology to investigate four classes of systematically perturbed derivatives of BLM to directly assess the effects on the Fe^{II} site due to variations of the ligand framework. The first class of derivatives (① in Figure 1) involves perturbations to the terminal amine substituent attached to the bithiazole: BLM mixture (Blenoxane), BLM A$_2$, BLM B$_2$, BLM demethyl A$_2$, and peplomycin (PEPLM). This functionality has generally been associated with facilitating DNA binding and is not expected to influence ligation at the metal center.[12] More recently, the bithiazole C-substituent has been modeled to fold underneath the metal binding domain on the same face as the hydroperoxide ligand in a HOO-Co^{III}BLM analogue and may influence the conformation at the metal

(55) Iitaka, Y.; Nakamura, H.; Nakatani, T.; Muraoka, Y.; Fujii, A.; Takita, T.; Umezawa, H. *J. Antibiot.* **1978**, *31*, 1070−1072.

(56) Sugiura, Y. *J. Antibiot.* **1978**, *31*, 1206−1208.

(57) Sugiura, Y.; Ishizu, K. *J. Inorg. Biochem.* **1979**, *11*, 171−180.

(58) Sugiura, Y.; Ishizu, K.; Miyoshi, K. *J. Antibiot.* **1979**, *32*, 453−461.

(59) Sugiura, Y. *J. Am. Chem. Soc.* **1980**, *102*, 5208−5215.

(60) Sugiura, Y.; Kuwahara, J.; Suzuki, T. *FEBS Lett.* **1985**, *182*, 39−42.

(61) Lehman, T. E.; Ming, L.-J.; Rosen, M. E.; Que, L., Jr. *Biochemistry* **1997**, *36*, 2807−2816.

(62) Oppenheimer, N. J.; Chang, C.; Chang, L.-H.; Ehrenfeld, G.; Rodriguez, L. O.; Hecht, S. M. *J. Biol. Chem.* **1982**, *257*, 1606−1609.

(63) Sugiura, Y.; Suzuki, T.; Otsuka, M.; Kobayashi, S.; Ohno, M.; Takita, T.; Umezawa, H. *J. Biol. Chem.* **1983**, *258*, 1328−1336.

(64) Akkerman, M. A. J.; Neijman, E. W. J. F.; Wijmenga, S. S.; Hilbers, C. W.; Bermel, W. *J. Am. Chem. Soc.* **1990**, *112*, 7462−7474.

(65) Arai, T.; Shinozuka, K.; Sawai, J. *Bioorg. Med. Chem. Lett.* **1997**, *7*, 15−18.

(66) Solomon, E. I.; Pavel, E. G.; Loeb, K. E.; Campochiaro, C. *Coord. Chem. Rev.* **1995**, *144*, 369−460.

(67) Whittaker, J. W.; Solomon, E. I. *J. Am. Chem. Soc.* **1988**, *110*, 5329−5339.

(68) Mabrouk, P. A.; Orville, A. M.; Lipscomb, J. D.; Solomon, E. I. *J. Am. Chem. Soc.* **1991**, *113*, 4053−4061.

(69) Pavel, E. G.; Martins, L. J.; Ellis, W. R., Jr.; Solomon, E. I. *Chem. Biol.* **1994**, *1*, 173−183.

(70) Pavlosky, M. A.; Zhang, Y.; Westre, T. E.; Gan, Q.-F.; Pavel, E. G.; Campochiaro, C.; Hedman, B.; Hodgson, K. O.; Solomon, E. I. *J. Am. Chem. Soc.* **1995**, *117*, 4316−4327.

(71) Loeb, K. E.; Westre, T. E.; Kappock, T. J.; Mitic, N.; Glasfeld, E.; Caradonna, J. P.; Hedman, B.; Hodgson, K. O.; Solomon, E. I. *J. Am. Chem. Soc.* **1997**, *119*, 1901−1915.

(72) Kasibhatla, B. T.; Loeb, K. E.; Westre, T. E.; Rodriguez, J. H.; Debrunner, P. G.; Hedman, B.; Hodgson, K. O.; Solomon, E. I.; Caradonna, J. P. Manuscript in preparation.

(73) Campochiaro, C.; Pavel, E. G.; Solomon, E. I. *Inorg. Chem.* **1995**, *34*, 4669−4675.

center.[42,43,74] The second group (oval in Figure 1) focuses on perturbations to the 3-*O*-carbamoyl substituent on the mannose sugar, the binding of which has long been a controversial topic in the field.[13] Within this class are *iso*-PEPLM and *iso*-BLM A₂ with the carbamoyl substituent shifted from the 3- to the 2-hydroxyl group of the mannose sugar of PEPLM or BLM A₂, respectively, as well as decarbamoyl-BLM A₂ for which the carbamoyl substituent has been eliminated. Electrochemical and EPR studies on Cu^{II}BLM derivatives indicate that ligation at the sixth site by the *O*-carbamoyl group contributes to the stability of the complex.[75] The third series (rectangle in Figure 1) addresses perturbations to the primary amine of the β-aminoalanine fragment: depyruvamide (DP)-PEPLM in which the β-aminoalamine moiety (and primary amine contained therein) is replaced with a H atom and *N*-acetyl-BLM A₂ in which the primary amine is made into a secondary amine through *N*-acetylation. Finally, although the acetamido side chain is not implicated in direct metal chelation,[76] the fourth class investigated involves epimerization at the α-methine carbon of the pyrimidine moiety of BLM A₂, which produces the opposite configuration (*R* instead of *S*) at C6 (Figure 1) linking the pyrimidine and secondary amine functionalities.

Azide and other small molecules bound to BLM have previously been shown to have similar spectroscopic properties as ethyl isocyanide bound to BLM, which is known to be a competitive inhibitor of dioxygen.[28,54] Thus, azide is used as a small molecule oxygen analogue to further probe the geometric and electronic structural features related to oxygenated BLM. In addition, the azide binding studies provide insight into the oxygen binding and reactivity of these complexes which can be correlated with their known DNA-cleaving capabilities. Derivatives in the first class with perturbations to the bithiazole C-substituent activate dioxygen and cleave DNA with similar efficiency and specificity as the natural product.[77,78] There is a 2- to 5-fold decrease in the efficiency, with a notable alteration in strand selectivity between multiple GC cleavage sites, for the class of derivatives having perturbations to the mannose sugar moiety.[22,78–81] More striking is the complete absence of DNA cleavage for DP-BLM, which lacks the primary amine of the β-aminoalanine fragment.[82] This complex forms a high-spin Fe^{III} species upon air oxidation, rather than the low-spin activated BLM of mechanistic relevance.[59] Similar behavior is also observed at low pH for deamido-BLM and synthetic models thereof[83] in which the carboxamido group of the β-aminoalanine moiety is hydrolyzed to an acid function by BLM hydrolase.[84] *N*-Acetylating the primary amine of the β-aminoalanine amide moiety (as in *N*-acetyl-BLM A₂) also

virtually eliminates all DNA strand scission; this has been attributed to an inability of the Fe^{II} complex to bind and/or reduce O₂.[85] Last, *epi*-P-3A shows a 3- to 5-fold decrease in cleavage efficiency relative to P-3A suggesting an important functional role of the acetamido side chain; this might involve metal ion binding, enhancing binding affinity or orientation with DNA, or sterically protecting the oxygen-binding pocket.[76,86]

In this paper we use low-temperature MCD spectroscopy in the d→d ligand field energy region to survey these series of derivatives as a probe of the empirical structural changes induced at the Fe^{II} active site by the extended ligand framework perurbations. Within each class, one member was chosen as a prototypical example for which more detailed VTVH MCD spectroscopy was pursued in order to assess the electronic effects associated with the modifications. In addition, azide binding to the various derivatives was monitored via CD, MCD, and VTVH MCD techniques to investigate the structural requirements of dioxygen binding to Fe^{II}BLM and to obtain further insight into the mechanism of dioxygen activation and DNA degradation. Finally, low-temperature absorption and MCD spectroscopies have been employed to study the CT bands in these complexes as a direct probe of the degree of Fe−pyrimidine π-interactions which can greatly influence the chemistry and reactivity of the derivatives relative to the unperturbed drug complex.

Experimental Section

Sample Preparation. Bleomycin sulfate (Blenoxane), a mixture of BLM A₂ (60%), BLM B₂ (30%), and other BLMs (∼10%), was obtained from Bristol-Meyers Squibb (Princeton, NJ). Blenoxane was fractionated[87] to afford BLM A₂, BLM B₂, and BLM demethyl A₂. BLM A₂ was converted to *iso*-BLM A₂,[88] *N*-acetyl-BLM A₂,[85,89] and *epi*-BLM A₂[90] as described. Decarbamoyl-BLM A₂ was prepared by total synthesis.[91] Individual BLM congeners were purified to homogeneity by C₁₈ reverse-phase HPLC; purity was verified by ¹H NMR spectroscopy. Peplomycin, *iso*peplomycin, and DP-peplomycin were obtained as purified species from Nippon Kayaku Co., Ltd. (Tokyo, Japan). ¹H NMR spectroscopy of *iso*peplomycin revealed the presence of a minor impurity not resolvable by C₁₈ reverse-phase HPLC.

Low-temperature absorption and MCD samples of Fe^{II}BLM and Fe^{II}-BLM derivatives were prepared as glasses in 50% (v/v) glycerol-*d₃* (98 atom % D; Aldrich) and 300 mM HEPES buffer (Sigma) dissolved in D₂O (99.9 atom % D; Aldrich) and adjusted to pD 8.2 with 40 wt % NaOD (Aldrich) in D₂O. For at least one derivative within each series for which low-temperature spectroscopy was performed, the presence of the glycerol glassing agent was verified to have no effect on the Fe^{II} d→d ligand field transitions via room-temperature CD spectroscopy. Also, the effect of cooling to He temperatures was shown to be minimal. All solutions were rigorously degassed with 8−10 freeze, pump, thaw cycles at 10⁻³ Torr in Teflon or ground glass stoppered flasks and immediately placed in a N₂ atmosphere (<10 ppm O₂). Solid forms of metal free BLMs and Fe(NH₄)₂(SO₄)₂·6H₂O (FeAS; MCB Manufacturing Chemists, Inc.) were evacuated and filled four times with Ar and solvated just prior to use in a N₂ atmosphere with buffered solution or D₂O, respectively. Fe^{II}BLM and Fe^{II}BLM deriva-

(74) Xu, R. X.; Nettesheim, D.; Otvos, J. D.; Petering, D. H. *Biochemistry* **1994**, *33*, 907−916.

(75) Ishizu, K.; Murata, S.; Miyoshi, K.; Suguira, Y.; Takita, T.; Umezawa, H. *J. Antibiot.* **1981**, *34*, 994−1000.

(76) Boger, D. L.; Honda, T.; Menezes, R. F.; Colletti, S. L.; Dang, Q.; Yang, W. *J. Am. Chem. Soc.* **1994**, *116*, 82−92.

(77) Kross, J.; Henner, W. D.; Hecht, S. M.; Haseltine, W. A. *Biochemistry* **1982**, *21*, 4310−4318.

(78) Sugiyama, H.; Kilkuskie, R. E.; Chang, L. H.; Ma, L.-T.; Hecht, S. M. *J. Am. Chem. Soc.* **1986**, *108*, 3852−3854.

(79) Shipley, J. B.; Hecht, S. M. *Chem. Res. Toxicol.* **1988**, *1*, 25−27.

(80) Boger, D. L.; Teramoto, S.; Honda, T.; Zhou, J. *J. Am. Chem. Soc.* **1995**, *117*, 7338−7343.

(81) Boger, D. L.; Teramoto, S.; Zhou, J. *J. Am. Chem. Soc.* **1995**, *117*, 7344−7356.

(82) Takahashi, K.; Ekimoto, H.; Aoyagi, S.; Koyu, A.; Kuramochi, H.; Yoshioka, O.; Matsuda, A.; Fujii, A.; Umezawa, H. *J. Antibiot.* **1979**, *32*, 36−42.

(83) Sugiyama, T.; Ohno, M.; Shibasaki, M.; Otsuka, M.; Sugiura, Y.; Kobayashi, S.; Maeda, K. *Bioorg. Med. Chem. Lett.* **1994**, *4*, 705−710.

(84) Sugiyama, T.; Ohno, M.; Shibasaki, M.; Otsuka, M.; Sugiura, Y.; Kobayashi, S.; Maeda, K. *Heterocycles* **1994**, *37*, 275−282.

(85) Oppenheimer, N. J.; Rodriguez, L. O.; Hecht, S. M. *Biochemistry* **1980**, *19*, 4096−4103.

(86) Boger, D. L.; Honda, T.; Menezes, R. F.; Colletti, S. L. *J. Am. Chem. Soc.* **1994**, *116*, 5631−5646.

(87) Chien, M.; Grollman, A. P.; Horwitz, S. B. *Biochemistry* **1977**, *16*, 3641−3646.

(88) Nakayama, Y.; Kunishima, M.; Omoto, S.; Takita, T.; Umezawa, H. *J. Antibiot.* **1973**, *26*, 400−402.

(89) Oppenheimer, N. J.; Rodriguez, L. O.; Hecht, S. M. *Biochemistry* **1979**, *18*, 3439−3445.

(90) Kunishima, M.; Fujii, T.; Nakayama, Y.; Takita, T.; Umezawa, H. *J. Antibiot.* **1976**, *29*, 853−856.

(91) An, H.; Katano, K.; Padmapriya, A. A.; Hess, C. D.; Hecht, S. M. Manuscript in preparation.

tives were prepared in the presence of 20% excess ligand by addition of a small aliquot of the FeAS stock solution to the metal free ligand in buffer/glycerol solution to give a final sample concentration of ~4 mM. Note that strictly anaerobic conditions were maintained throughout this procedure so that the additional use of reducing agents could be avoided as dithionite was determined to significantly affect the observed spectral features. The samples were syringed into a 0.3 cm path length MCD cell assembled under a N_2 atmosphere with a neoprene spacer sandwiched between two Infrasil quartz disks. The samples were quick frozen in liquid N_2 (LN_2) and inserted into the cryostat under a high flow of He gas. Room-temperature CD samples were prepared in a similar fashion with the omission of the glycerol-d_3. The samples were maintained anaerobic in a 0.5 or 1.0 cm path length cuvette specially adapted with a Kontes stopcock seal. For the azide binding studies, sodium azide (NaN_3; Aldrich) solutions (in D_2O) were prepared at various concentrations to minimize the effects of dilution on the BLM samples. The solutions were prepared following similar anaerobic techniques as previously described. The anaerobic CD cell was brought into the N_2-filled glovebox for each azide addition during the titrations and a 5 in. needle was used to reach the bottom of the cell to ensure complete mixing. The azide-bound samples for MCD were prepared by adding a small aliquot of NaN_3 solution to the $Fe^{II}BLM$ or Fe^{II}-BLM derivatives to give the desired final molar ratio of N_3^- to Fe. Sufficient mixing was performed to ensure that the reactions were complete before the samples were loaded into the MCD cells and frozen.

Ligand Field Region CD/MCD Instrumentation. Room-temperature NIR CD spectra (278 K, 600−2000 nm) were obtained with a Jasco 200D spectropolarimeter interfaced to a Power Macintosh 7100/66 computer and a LN_2-cooled InSb detector. The sample temperatures were maintained by a recirculating water bath kept just below 278 K. Data acquisition was achieved by using routines written within the software package LabVIEW (National Instruments). Contributions to the CD intensity due to buffer and cell backgrounds were subtracted from the sample CD spectra. Low-temperature NIR MCD spectra (1.6−100 K, 600−2000 nm) were obtained with the Jasco 200D spectropolarimeter and an Oxford Instruments SM4000-7 T superconducting magnet/cryostat. Depolarization of all frozen samples (<10%) was measured by monitoring the CD intensity of a nickel (+)-tartrate solution placed before and after the sample chamber.[92] MCD spectra were corrected for zero-field baseline effects induced by cracks in the glasses by subtracting the corresponding 0 T scan at each temperature.

Charge-Transfer Region Absorption/MCD Instrumentation. Low-temperature UV/vis absorption spectra (5 K, 300−900 nm) were recorded on a Cary 17 UV/vis spectrophotometer equipped with a Janis Super Varitemp helium cryostat and interfaced to a Compaq 386 computer with OLIS software. Residual absorption due to buffer, glycerol, or glass scattering effects was subtracted from all of the spectra. Low-temperature UV/vis MCD spectra (5−100 K, 300−900 nm) were obtained on a Jasco 500C spectropolarimeter with an extended S-20 photomultiplier tube (Hammamatsu), interfaced to a Macintosh IIvx computer, and equipped with an Oxford SM4-7T magnet/cryostat. All absorption, CD, and MCD spectra were smoothed by using a weighted fitting routine and resolved into Gaussian band shapes with use of a constrained nonlinear least-squares fitting protocol.

Results and Analysis

A. Ligand Field Region. 1. Excited-State Spectral Comparison. The 5 K, 7 T NIR MCD spectra of $Fe^{II}PEPLM$, $Fe^{II}iso$-PEPLM, $Fe^{II}DP$-PEPLM, and $Fe^{II}epi$-BLM A_2 are shown in Figure 2 with the Gaussian resolved energies summarized in Table 1. The MCD spectrum of $Fe^{II}PEPLM$ (Figure 2A) is nearly identical with that of $Fe^{II}BLM$ (Blenoxane mixture)[52] as well as other derivatives ($Fe^{II}BLM$ A_2, $Fe^{II}BLM$ B_2, and Fe^{II}-BLM demethyl A_2) having structurally altered C-terminal amine substituents (see Supporting Information); this indicates that differences in the chemical nature and charge of the terminus
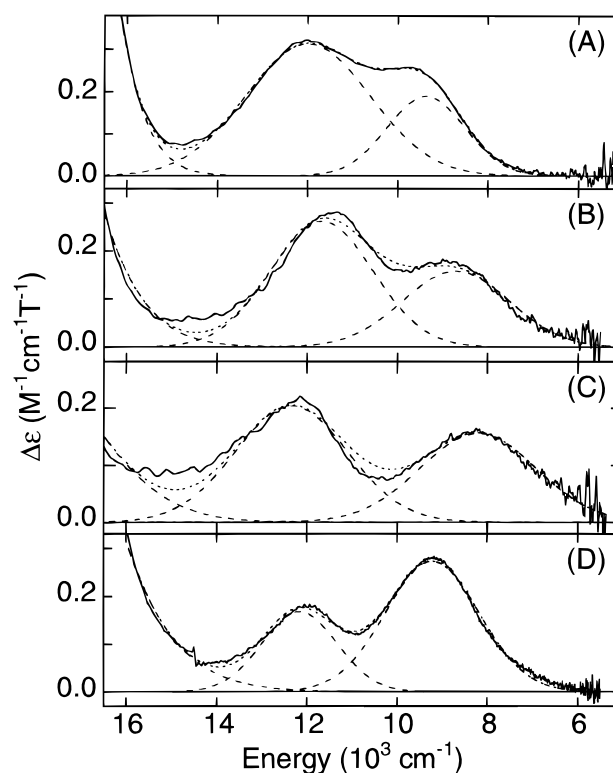
(92) Browett, W. R.; Fucaloro, A. F.; Morgan, T. V.; Stephens, P. J. *J. Am. Chem. Soc.* **1983**, *105*, 1868−1872.

Figure 2. MCD spectra (—) at 5 K and 7 T for (A) $Fe^{II}PEPLM$, (B) $Fe^{II}iso$-PEPLM, (C) $Fe^{II}DP$-PEPLM, and (D) $Fe^{II}epi$-BLM A_2. Each plot includes the Gaussian resolution fit (···) to the data and individual components (− −). The energies of the transitions are summarized in Table 1.

have no effect on the energies or splittings of the NIR d→d transitions. In contrast, the $Fe^{II}iso$-PEPLM MCD spectrum (Figure 2B) indicates two Fe^{II} ligand field d→d transitions which are shifted to significantly lower energy ($10Dq = 10\,190$ cm^{-1}) relative to those for $Fe^{II}PEPLM$ ($10Dq = 10\,685$ cm^{-1}) indicating a weaker ligand field strength at the Fe^{II} site. Similar spectral features are observed for $Fe^{II}iso$-BLM A_2 and upon removal of the 3-O-carbamoyl substituent in Fe^{II}decarbamoyl-BLM A_2 (see Supporting Information). Thus shifting the carbamoyl substituent from the 3- to the 2-hydroxyl position of the mannose sugar or eliminating it entirely perturbs the structure of the Fe^{II} site and provides evidence that either the carbamoyl functionality itself is a metal-binding ligand or it is in close association with an active site ligand resulting in a second coordination sphere conformational effect. Even more dramatic is the increased excited-state splitting of 4150 cm^{-1} observed in the MCD spectrum of $Fe^{II}DP$-PEPLM (Figure 2C). This is significantly larger than the splittings observed for Fe^{II}-PEPLM (2630 cm^{-1}) and $Fe^{II}iso$-PEPLM (2980 cm^{-1}) and suggests a very weak sixth axial interaction; the five-coordinate limiting structure would have a splitting of 5000 cm^{-1}. Thus removing the β-aminoalanine moiety alters the structure of the Fe^{II} site and identifies the primary amine functionality as contributing directly to metal binding. Altering the binding properties of the primary amine through N-acetylation (in $Fe^{II}N$-acetyl-BLM A_2) results in similar spectral features (see Supporting Information). The Gaussian resolution of the low-temperature MCD spectrum of $Fe^{II}epi$-BLM A_2 is plotted in Figure 2D. Although the energies of the transitions are nearly identical with those observed for $Fe^{II}BLM$ (Table 1), the intensity ratio is reversed. Thus, changing the stereochemistry at C6 linking the pyrimidine and secondary amine ligands does

Table 1. Fe^{II}BLM and Fe^{II}BLM Derivative Ligand Field Transition Energies, Excited-State Splittings, and Ligand Field Strengths

complex	CD/MCD	energy of band 1 (cm^{-1})	energy of band 2 (cm^{-1})	Δ^5E_g (cm^{-1})	$10Dq$ (cm^{-1})
Fe^{II}BLM	MCD	9410	12 050	2640	10 730
Fe^{II}BLM A$_2$	MCD	9460	12 095	2635	10 780
Fe^{II}BLM B$_2$	MCD	9400	12 000	2600	10 700
Fe^{II}BLM deMe A$_2$	MCD	9230	12 030	2800	10 630
Fe^{II}PEPLM	CD	9100	13 050	3950	11 075
	MCD	9370	12 000	2630	10 685
Fe^{II}*iso*-PEPLM	CD	7500, 9000	12 050	3050	10 525
	MCD	8700	11 680	2980	10 190
Fe^{II}*iso*-BLM A$_2$	MCD	8690	11 420	2730	10 055
Fe^{II}decarbamoyl-BLM A$_2$	MCD	8470	11 520	3050	9995
Fe^{II}DP-PEPLM	CD	8400	12 500	4100	10 450
	MCD	8200	12 350	4150	10 275
Fe^{II}*N*-acetyl-BLM A$_2$	MCD	8470	12 385	3915	10 430
Fe^{II}*epi*-BLM A$_2$	CD	8500	12 800	4300	10 650
	MCD	9210	12 160	2950	10 685
Fe^{II}BLM + N$_3^-$	CD	9100	12 000	2900	10 550
	MCD	9350	12 500	3150	10 925
Fe^{II}*iso*-PEPLM + N$_3^-$	CD	9100	12 000	2900	10 550
	MCD	9170	12 060	2890	10 615
Fe^{II}DP-PEPLM + N$_3^-$	CD	7400	12 200	4800	9800
	MCD	8000	12 200	4200	10 100
Fe^{II}*epi*-BLM A$_2$ + N$_3^-$	CD	8700	11 900	3200	10 300
	MCD	9020	12 280	3260	10 650

not significantly affect the ligand field strength at the Fe^{II} site but does appear to change the mixing of the wave functions.

2. Determination of Ground-State Parameters. To further investigate the effects of perturbations to the terminal amine moiety, VTVH MCD spectroscopy was pursued on Fe^{II}PEPLM as the prototype example from this class of derivatives. VTVH MCD data were collected on both ligand field d→d transitions and give quantitatively identical results. The data collected at 12 000 cm^{-1} are plotted in Figure 3A as a function of the reduced parameter $\beta H/2kT$ for a series of fixed temperatures. The lowest temperature data are well fit assuming a $-D$ model in which the observed nesting behavior results from rhombic ZFS (δ) of the $M_s = \pm 2$ non-Kramers doublet ground state. The experimentally determined ground-state parameters are $\delta = 2.4$ cm^{-1}, $g_{\parallel} = 9.3$ and a very small off-axis Zeeman contribution with a polarization ratio M_z/M_{xy} of -0.04. This value of δ (also observed for Fe^{II}BLM) is unusually low for a six-coordinate complex and has been attributed to strong π-back-bonding interactions with the pyrimidine ligand.[52] Applying this fit to the full temperature set and allowing for potential thermal population of low-lying excited states places the lowest component of the $M_s = \pm 1$ level at an energy (E_S) 35 cm^{-1} above the ground state. Using correlation diagrams produced from the full solution to the $^5T_{2g}$ Hamiltonian[66] to relate the ground-state spin Hamiltonian values of δ and $g_{\parallel}$ to the axial and rhombic ligand field parameters gives $\Delta = -900 \pm 100$ cm^{-1} and $|V/2\Delta| = 0.16$. These values are nearly identical with those obtained previously for Fe^{II}BLM and are summarized in Table 2.

VTVH MCD spectroscopy was pursued on Fe^{II}*iso*-PEPLM as the representative derivative for the class of complexes with variations to the carbamoyl substituent on the mannose sugar. Data were collected on both ligand field bands and are plotted for the 12 000 cm^{-1} transition in Figure 3B. Qualitatively, the data are significantly more nested than those observed for Fe^{II}-PEPLM (Figure 3A). The lowest temperature data are well fit assuming a $-D$ model with $\delta = 4.8$ cm^{-1} and $g_{\parallel} = 9.0$. There is a sizable off-axis Zeeman contribution with a polarization ratio M_z/M_{xy} of -0.13 (0.03 for the 8500 cm^{-1} band) and a $\mathcal{B}$-term contribution of 3% (1% for the 8500 cm^{-1} band). Applying this fit to the full temperature set places the lowest
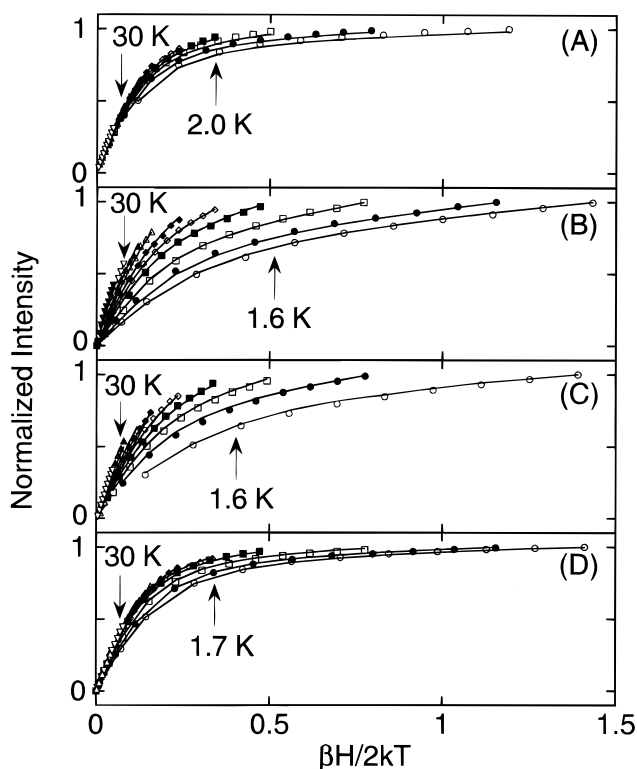

Figure 3. Variable-temperature variable-field saturation magnetization data for (A) Fe^{II}PEPLM recorded at 12 000 cm^{-1}, (B) Fe^{II}*iso*-PEPLM recorded at 12 000 cm^{-1}, (C) Fe^{II}DP-PEPLM recorded at 12 350 cm^{-1}, and (D) Fe^{II}*epi*-BLM A$_2$ recorded at 9200 cm^{-1}. The MCD intensity is normalized and plotted (symbols) as a function of $\beta H/2kT$ for a series of fixed temperatures (1.6 to 50 K) and magnetic fields (0 to 7 T). The fits (solid lines) to the VTVH MCD data were generated from the parameters given in Table 2. Errors in the data points are smaller than the symbol size used.

component of the $M_s = \pm 1$ excited state above the thermal range of the experiment and is consistent with the $-D$ interpretation. Relating the ground-state spin Hamiltonian values of δ and $g_{\parallel}$ to the axial and rhombic ligand field parameters gives $\Delta = -600 \pm 100$ cm^{-1} and $|V/2\Delta| = 0.32$ (Table 2). Similar VTVH MCD data were obtained for Fe^{II}*iso*-BLM A$_2$ in this energy region.

Table 2. Fe^{II}BLM and Fe^{II}BLM Derivative Ground-State Spin Hamiltonian and Ligand Field Parameters

complex	δ (cm^{-1})	$g_{\parallel}$	M_z/M_{xy}	E_S (cm^{-1})	Δ (cm^{-1})	$|V/2\Delta|$	V (cm^{-1})
Fe^{II}BLM	2.4	9.3	−0.04		−800 ± 100	0.18	280 ± 50
Fe^{II}PEPLM	2.4	9.3	−0.04	35	−900 ± 100	0.16	280 ± 50
Fe^{II}*iso*-PEPLM	4.8	9.0	−0.13		−600 ± 100	0.32	380 ± 70
Fe^{II}DP-PEPLM	4.4	9.2		22	−600 ± 50	0.33	400 ± 50
Fe^{II}*epi*-BLM A$_2$	2.6	9.4	−0.10	28	−800 ± 100	0.15	240 ± 60
Fe^{II}BLM + N$_3^-$	3.1	9.2	0.01		−750 ± 100	0.22	330 ± 50
Fe^{II}*iso*-PEPLM + N$_3^-$	2.4	9.2	−0.10		−900 ± 100	0.22	400 ± 80

In both cases variation in the carbamoyl moiety produces a significant change on the Fe^{II} ground state.

VTVH MCD data were collected for Fe^{II}DP-PEPLM on both ligand field d→d transitions and give qualitatively identical results. The data collected at 12 350 cm^{-1} are plotted in Figure 3C as a function of the reduced parameter $\beta H/2kT$ for a series of fixed temperatures. The lowest temperature data are well fit assuming a $-D$ model with δ = 4.4 cm^{-1} and $g_{\parallel}$ = 9.2. This value of δ is again significantly larger (data are more nested) than observed for Fe^{II}PEPLM (δ = 2.4 cm^{-1}) and on the order obtained for Fe^{II}*iso*-PEPLM (δ = 4.8 cm^{-1}). Applying this fit to the full temperature set places the lowest component of the $M_s = \pm 1$ excited state at 22 cm^{-1} above the ground state. Relating the ground-state spin Hamiltonian values of δ and $g_{\parallel}$ to the axial and rhombic ZFS parameters gives $\Delta = -600 \pm 50$ cm^{-1} and $|V/2\Delta|$ = 0.33. As the energies of the $S = 2$ spin sublevels for $+D$ and $-D$ systems converge at the rhombic limit,[66] this splitting pattern is consistent with both $+D$ and $-D$ models and is equally well described with $D = 11.0 \pm 1.0$ and $E = 2.9 \pm 0.3$. For comparison to the other derivatives investigated thus far which can only be fit with a $-D$ model, the corresponding values of $-\Delta$ and $|V/2\Delta|$ for Fe^{II}DP-PEPLM are summarized in Table 2. Note that VTVH MCD data were also collected on the Fe^{II}*N*-acetyl-BLM A$_2$ sample and show similar behavior.

For Fe^{II}*epi*-BLM A$_2$ the VTVH MCD data collected at 9200 cm^{-1} are plotted in Figure 3D as a function of the reduced parameter $\beta H/2kT$ for a series of fixed temperatures. The lowest temperature data are well fit assuming a $-D$ model with δ = 2.6 cm^{-1} and $g_{\parallel}$ = 9.4 with a small off-axis Zeeman contribution (M_z/M_{xy}) of -0.10. Applying this fit to the full temperature set and allowing for potential thermal population of low-lying excited states places the lowest component of the $M_s = \pm 1$ excited state at 28 cm^{-1} above the ground state. Relating the ground-state spin Hamiltonian values of δ and $g_{\parallel}$ to the axial and rhombic ZFS parameters gives $\Delta = -800 \pm 100$ cm^{-1} and $|V/2\Delta|$ = 0.15 which are of similar magnitude to those values obtained previously for Fe^{II}BLM and are summarized in Table 2. Thus, changing the stereochemistry at C6 linking the pyrimidine and secondary amine ligands does not significantly affect the Fe^{II} ground-state parameters.

3. Azide Binding Studies. Figure 4A shows the room-temperature CD spectra for Fe^{II}BLM upon addition of 0, 0.5, 1.0, 1.5, 2.8, 5.2, 7.4, 13, 20, 43, and 86 molar equiv of NaN$_3$. The original spectrum with two positive CD bands changes to a new spectrum with one positive and one negative band as summarized in Table 1. In addition a more intense charge-transfer transition grows in at higher energy ($\sim$16 000 cm^{-1}). The reaction appears to be complete at 43 equiv of N$_3^-$ as there is no change in the intensity of the two Fe^{II} ligand field d→d transitions between the 43 and 86 equiv spectra. A ratio as large as 320-fold was investigated with no evidence for further
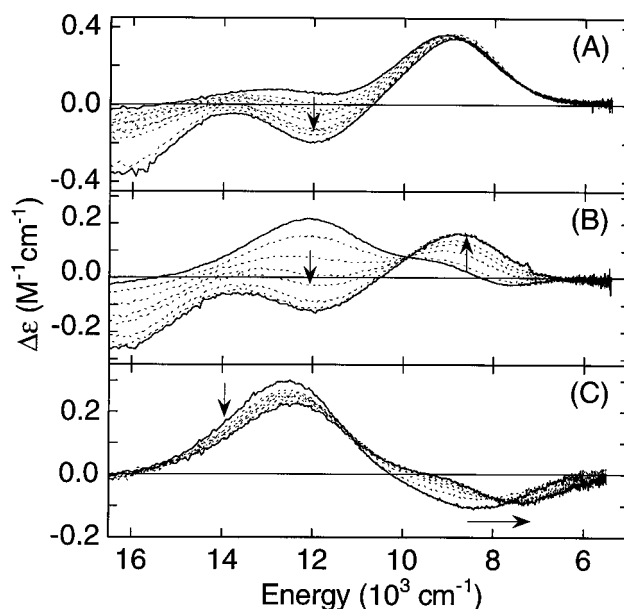

Figure 4. CD spectra recorded at 278 K for (A) Fe^{II}BLM in the presence of 0, 0.5, 1.0, 1.5, 2.8, 5.2, 7.4, 13, 20, 43, and 86 equiv of N$_3^-$, (B) Fe^{II}*iso*-PEPLM in the presence of 0, 1.0, 3.5, 7.5, 12, 27, 47, and 82 equiv of N$_3^-$, and (C) Fe^{II}DP-PEPLM in the presence of 0, 1.0, 3.5, 7.5, 12, 27, 47, and 82 equiv of N$_3^-$. The energies of the transitions are summarized in Table 1.

reaction. A Scatchard[93] analysis of the titration data yields an azide binding affinity for Fe^{II}BLM of 60.1 ± 3.6 M^{-1}. A similar titration was carried out for azide binding to Fe^{II}PEPLM to investigate the potential implications on small molecule reactivity associated with perturbations to the terminal amine moiety attached to the bithiazole. Equivalent data were obtained with a comparable binding constant of $\sim$67.2 M^{-1}. Thus if the bithiazole C-substituent is folded underneath the metal-binding domain,[13,94] the functionality on the terminus does not affect the accessibility of the metal site to exogenous ligands.

Figure 4B shows the room-temperature CD spectra for Fe^{II}*iso*-PEPLM in the presence of 0, 1.0, 3.5, 7.5, 12, 27, 47, and 82 molar equiv of NaN$_3$. The CD spectrum in the absence of azide is drastically different from that of BLM/PEPLM. Two dominant bands are observed at 9 000 and 12 050 cm^{-1} which are at similar energies to the corresponding MCD transitions which identifies them as the d→d bands. There is an additional weak negative feature at 7500 cm^{-1}, which varies in intensity between Fe^{II}*iso*-PEPLM and Fe^{II}*iso*-BLM A$_2$ and can be associated with the second minor ligand component seen in the NMR analysis. This change in the Fe^{II} site in the *iso* derivatives does not appear to affect small molecule binding as addition of azide changes the spectrum to one closely resembling that

(93) Connors, K. A. *Binding Constants*; John Wiley & Sons: New York, 1987.
(94) Petering, D. H.; Mao, Q.; Li, W.; DeRose, E.; Antholine, W. E. *Metal Ions in Biological Systems*; Sigel, A., Sigel, H., Eds.; Marcel Dekker: Inc.: New York, 1996; Vol. 33, pp 619−648.

observed for Fe^{II}BLM + N$_3^-$ (Figure 4A) with one lower energy positive band (at 9100 cm^{-1}) and one higher energy negative band (at 12 000 cm^{-1}). Thus either a coordination position occupied by the bound carbamoyl ligand in Fe^{II}BLM is the exchangeable site of small molecule binding or a second coordination sphere geometric constraint induced by the carbamoyl substituent on an Fe^{II} ligand is eliminated upon replacing the weak solvent molecule with the dioxygen analogue. The azide binding reaction of Fe^{II}*iso*-PEPLM appears to be complete at 47 equiv of N$_3^-$ as there is no change in the intensity of the two new transitions between the 47 and 82 equiv spectra. A Scatchard[93] analysis results in a single equilibrium binding constant of 25.2 ± 0.5 M^{-1}. This is more than a factor of 2 lower than that determined for the unperturbed Fe^{II}BLM complex. Note that similar CD spectra were also obtained for Fe^{II}*iso*-BLM A$_2$ and Fe^{II}decarbamoyl-BLM A$_2$ in the absence and presence of 80 molar equiv of N$_3^-$.

The room-temperature CD spectra for Fe^{II}DP-PEPLM in the presence of 0, 1.0, 3.5, 7.5, 12, 27, 47, and 82 molar equiv of NaN$_3$ are shown in Figure 4C. In the absence of azide there is an increased splitting of the d→d bands relative to those for Fe^{II}BLM (3950 to 4100 cm^{-1}) with a change in sign of the lower energy transition. Upon addition of the small molecule there is very little change in the Fe^{II}DP-PEPLM spectral features; the lower energy band moves even lower (8400 to 7400 cm^{-1}) and the intensity and energy of the higher energy feature decrease slightly (12 500 to 12 200 cm^{-1}). The CD spectrum of Fe^{II}DP-PEPLM + N$_3^-$ is very different from that observed for Fe^{II}BLM + N$_3^-$ (Figure 4A) and Fe^{II}*iso*-PEPLM + N$_3^-$ (Figure 4B) and suggests that a different Fe^{II} ligand set is involved in the azide-bound DP-PEPLM complex. A Scatchard[93] analysis for the titration of Fe^{II}DP-PEPLM with N$_3^-$ yields a binding constant of 29.7 ± 5.2 M^{-1}. This is roughly a factor of 2 lower than that determined for the unperturbed Fe^{II}BLM complex and of the same magnitude as that determined for the Fe^{II}*iso*-PEPLM complex. CD spectra were also collected for Fe^{II}*N*-acetyl-BLM A$_2$ in the absence and presence of an 80-fold molar excess of N$_3^-$. The intensity ratio of the transitions both before and after azide addition is slightly perturbed but the actual energies of the transitions are quite comparable.

The two similar azide-bound complexes of BLM/PEPLM and *iso*-PEPLM were further investigated by using low-temperature MCD spectroscopy. The 5 K, 7 T MCD spectra of Fe^{II}BLM (solid line) and Fe^{II}*iso*-PEPLM (dashed line) each with an 80-fold molar excess of N$_3^-$ are shown in Figure 5A. For Fe^{II}BLM + N$_3^-$ two Fe^{II} ligand field d→d transitions are observed at 9 350 and 12 500 cm^{-1} (Table 1). There is a shoulder near 11 500 cm^{-1} that could result from uncomplexed Fe^{II}BLM in solution. However, based on the room-temperature binding constant determined from the CD titration, less than 6% of the sample is expected to be unbound under these experimental conditions, which is too small to account for the observed intensity; and in fact, an Fe^{II}BLM sample containing only a 5-fold molar excess of N$_3^-$ displayed an MCD spectrum that was virtually superimposable with that of the 80-fold excess sample. Thus the shoulder is not attributed to unconverted Fe^{II}BLM and perhaps arises from a minor BLM congener present in the Blenoxane mixture. The MCD spectrum for Fe^{II}*iso*-PEPLM + N$_3^-$ also shows two transitions at 9 170 and 12 060 cm^{-1} with a shoulder near 11 500 cm^{-1}. There is a slight decrease in the energies of the two dominant transitions and small variation in the ratio of their intensities compared with that of Fe^{II}BLM + N$_3^-$, but the overall shapes of the spectra are quite similar, indicating equivalent first coordination sphere

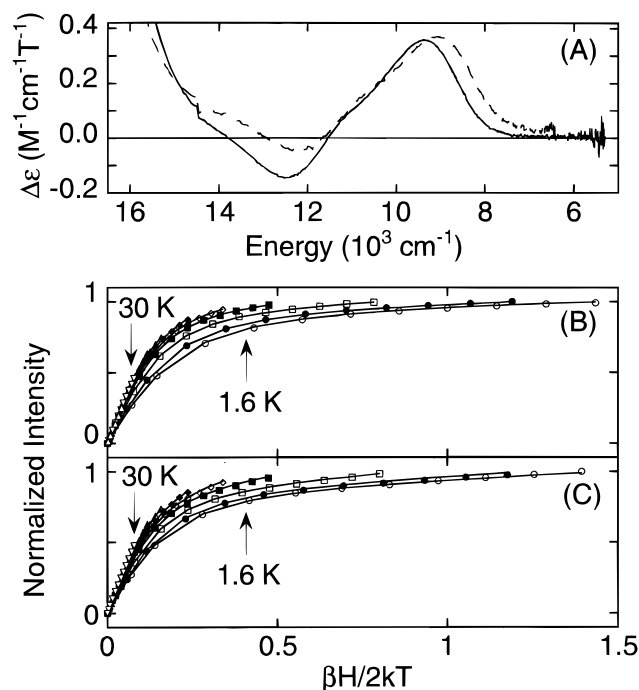**Figure 5.** (A) MCD spectra at 5 K and 7 T for Fe^{II}BLM + N$_3^-$ (—) and Fe^{II}*iso*-PEPLM + N$_3^-$ (— —). Variable-temperature variable-field saturation magnetization data for (B) Fe^{II}BLM + N$_3^-$ recorded at 9185 cm^{-1} and (C) Fe^{II}*iso*-PEPLM + N$_3^-$ recorded at 8900 cm^{-1}. For both samples the MCD intensity is normalized and plotted (symbols) as a function of $\beta H/2kT$ for a series of fixed temperatures (1.6 to 30 K) and magnetic fields (0 to 7 T). The fits (solid lines) to the VTVH MCD data were generated from the parameters given in Table 2. Errors in the data points are smaller than the symbol size used.

environments. The additional shoulder in the Fe^{II}*iso*-PEPLM + N$_3^-$ spectrum is attributed to a minor component evident from the ^{1}H NMR analysis.

To further evaluate whether the azide-bound forms of Fe^{II}-BLM and Fe^{II}*iso*-PEPLM are indeed structurally equivalent, as appears to be the case based on their similar room-temperature CD and low-temperature MCD spectra, VTVH MCD data were collected at 9185 cm^{-1} for Fe^{II}BLM + N$_3^-$ and 8900 cm^{-1} for Fe^{II}*iso*-PEPLM + N$_3^-$ and are plotted in Figure 5, spectra B and C, respectively, as a function of the reduced parameter $\beta H/2kT$. Qualitatively the data look very similar and are virtually superimposable. For Fe^{II}BLM + N$_3^-$ the lowest temperature data are well fit by using a $-D$ model with $\delta = 3.1$ cm^{-1}, $g_{||} = 9.2$, and a very small off-axis Zeeman contribution with a polarization ratio M_z/M_{xy} of 0.01. These ground-state spin Hamiltonian values of δ and $g_{||}$ are related to the axial and rhombic ligand field parameters and give $\Delta = -750 \pm 100$ cm^{-1} and $|V/2\Delta| = 0.22$ as summarized in Table 2. For Fe^{II}*iso*-PEPLM + N$_3^-$ the lowest temperature data are also well fit by using a $-D$ model with $\delta = 2.4$ cm^{-1}, $g_{||} = 9.2$, and a small off-axis Zeeman contribution with a polarization ratio M_z/M_{xy} of -0.10. The resulting axial and rhombic ligand field parameters are $\Delta = -900 \pm 100$ cm^{-1} and $|V/2\Delta| = 0.22$, which compare favorably with those observed for Fe^{II}BLM + N$_3^-$.

B. Charge-Transfer Region. The low-temperature UV/vis absorption and MCD spectra for Fe^{II}PEPLM, Fe^{II}*iso*-PEPLM, Fe^{II}DP−PEPLM, and Fe^{II}*epi*-BLM A$_2$ are shown in Figure 6A−D, respectively. The absorption and MCD spectra for Fe^{II}-PEPLM show two envelopes of transitions that can be simultaneously Gaussian resolved into five bands at 18 050, 20 335, 22 700, 25 860, and 28 330 cm^{-1}. These energies are nearly
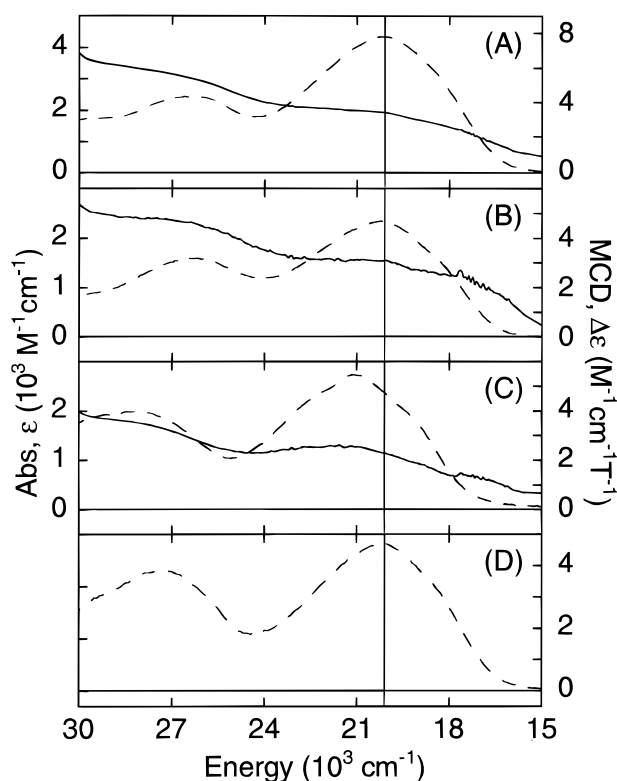
Figure 6. Charge-transfer region absorption spectra (—) at 5 K and MCD spectra (− −) at 5 K and 7 T for (A) Fe^{II}BLM, (B) Fe^{II}*iso*-PEPLM, (C) Fe^{II}DP-PEPLM, and (D) Fe^{II}*epi*-BLM A$_2$ (MCD spectrum only).

Table 3. Fe^{II}BLM and Fe^{II}BLM Derivative Charge Transfer Transition Energies (cm^{-1})

complex	band 1	band 2	band 3	band 4	band 5
Fe^{II}BLM	18 100	20 350	22 690	26 040	29 000
Fe^{II}BLM A$_2$	18 640	19 970	22 510	25 820	28 120
Fe^{II}BLM B$_2$	18 820	19 900	22 680	25 810	28 230
Fe^{II}BLM deMe A$_2$	18 510	20 660	23 330	26 140	28 550
Fe^{II}PEPLM	18 050	20 335	22 700	25 860	28 330
Fe^{II}*iso*-PEPLM	18 000	20 130	22 500	25 870	28 400
Fe^{II}*iso*-BLM A$_2$	18 950	20 610	22 585	25 640	28 325
Fe^{II}decarbamoyl-BLM A$_2$	18 120	19 785	21 610	25 160	27 430
Fe^{II}DP−PEPLM	19 680	21 400	23 450	27 120	29 000
Fe^{II}N-acetyl-BLM A$_2$	19 740	21 270	22 990	27 030	29 970
Fe^{II}*epi*-BLM A$_2$	18 340	20 140	22 170	26 930	29 750

identical with those observed previously for Fe^{II}BLM and assigned as Fe^{II} d$_\pi$→pyrimidine π^* MLCT transitions.[52] The variations to the terminal amine moiety of the bithiazole have little effect on these low-energy MLCT transitions, the energies of which are summarized in Table 3 for Fe^{II}BLM, Fe^{II}BLM A$_2$, Fe^{II}BLM B$_2$, Fe^{II}BLM demethyl A$_2$, and Fe^{II}PEPLM. Similarly, the absorption and MCD spectra for Fe^{II}*iso*-PEPLM (Figure 6B) show the same five Gaussian resolved bands at 18 000, 20 130, 22 500, 25 870, and 28 400 cm^{-1}. Similar transition energies (Table 3) for the other derivatives with perturbations to the carbamoyl substituent on the mannose sugar, Fe^{II}*iso*-BLM A$_2$ and Fe^{II}decarbamoyl-BLM A$_2$, suggest that the presence of the carbamoyl ligand has little impact on the charge-transfer spectroscopy of resting BLM.[52] As these CT bands were assigned as Fe^{II} d$_\pi$→pyrimidine π^* MLCT transitions the Fe−pyrimidine bond is therefore not affected by this sugar modification. Figure 6C shows the absorption and MCD spectra for Fe^{II}DP-PEPLM. There is clearly evident a shift in the positions of the maxima of both transition envelopes of ~1000 cm^{-1} to higher energy. The Fe^{II}DP-PEPLM (and similarly the

Fe^{II}N-acetyl-BLM A$_2$) spectra can be simultaneously Gaussian resolved (Table 3) into five low-energy MLCT transitions at 19 680, 21 400, 23 450, 27 120, and 29 000 cm^{-1}. This shift to higher energy indicates that removing the primary amine ligand or hindering its ability to coordinate to the metal affects the electronic structure at the Fe^{II} site, resulting in weakened π-interactions with the pyrimidine. The MCD spectrum for Fe^{II}*epi*-BLM A$_2$ is shown in Figure 6D and can be fit to five Gaussian bands at 18 340, 20 140, 22 170, 26 930, and 29 750 cm^{-1} (Table 3). The lower energy envelope occurs at approximately the same energy as in the unperturbed BLM mixture although the higher energy envelope is shifted slightly.

Discussion

Despite numerous attempts to characterize the endogenous ligand set in Fe^{II}BLM, the lack of available spectroscopic techniques for high-spin ferrous systems, which has led most studies to focus on different metal-substituted and ligand-bound forms of BLM, coupled with the complexity of the ligand framework have made such determinations difficult and a well-defined first coordination sphere is still being developed. We have sought to address this issue by using MCD spectroscopy applied to a series of systematically altered derivatives. In particular we have investigated four classes of compounds with variations to the terminal amine attached to the bithiazole, the carbamoyl substituent on the mannose sugar, the primary amine of the β-aminoalanine fragment, and the stereochemistry at the α-methine carbon of the pyrimidine moiety. The terminal amine plays no role in metal chelation or in conformationally affecting the first coordination sphere of the metal as there is no difference in the Fe^{II} ligand field MCD spectra of a variety of derivatives differing only in the charge and chemical nature of this functionality. In each case, the spectroscopy is consistent with a six-coordinate, distorted octahedral geometry at the Fe center as previously observed for the unmodified form.[52]

Direct coordination of the 3-O-carbamoyl substituent on the mannose sugar is the most straightforward explanation of the different Fe^{II} ligand field strengths (10Dq) observed in the MCD spectra of Fe^{II}*iso*-PEPLM, Fe^{II}*iso*-BLM A$_2$, and Fe^{II}decarbamoyl-BLM A$_2$ relative to Fe^{II}BLM and Fe^{II}PEPLM. Coordination of the carbonyl oxygen of the carbamoyl can account for the weak axial ligand in the resting structure; it has been proposed in one study[75] of Cu^{II}BLM and occurs in the crystallographically characterized Ni^{II} complex of N,N'-bis(2-carbamoylethyl)-ethylenediamine.[95] The possibility of amide coordination of the carbamoyl seems less likely as this would require deprotonation; its pK_a is ~13 and competition of the high-spin Fe^{II} ion with the proton for the free base is expected to lower this by at most several log units.[96] An alternative explanation of the differences in the ligand field spectra for these derivatives would be a second coordination sphere perturbation of an active site ligand as a result of the sugar modifications, and not from a direct ligand substitution effect (vide infra). If that were the case, the same conformational change might be expected to manifest itself in the spectral features of the azide-bound complexes; however, this is not observed.

The Fe^{II} ligand field MCD spectra for Fe^{II}DP-PEPLM and Fe^{II}N-acetyl-BLM A$_2$ show an increased splitting (Δ^5E_g) of the two Fe^{II} d→d MCD transitions relative to Fe^{II}PEPLM and Fe^{II}-BLM A$_2$, indicating that removing or perturbing the primary

(95) Hay, R. W.; Perotti, A.; Oberti, R.; Ungaretti, L. *Transition Met. Chem.* **1993**, *18*, 570−572.

(96) Holm, R. H.; Kennepohl, P.; Solomon, E. I. *Chem. Rev. (Washington, D.C.)* **1996**, *96*, 2239−2314.

amine of the β-aminoalanine amide moiety greatly affects the Fe^{II} coordination sphere and unambiguously identifies it as a metal-chelating ligand. Changing the stereochemistry at C6 linking the pyrimidine and secondary amine functionalities affects the ligand field d→d band positions in the room-temperature CD spectrum and the intensity ratio of the transitions, not their energies or splitting, in the MCD spectrum for $Fe^{II}epi$-BLM A$_2$ relative to Fe^{II}BLM A$_2$, suggesting that the stereochemical perturbation has only a small affect on the excited-state orbital wave functions but not the actual ligand set at the Fe^{II} site.

Thus MCD spectroscopy, which directly probes ligand variations at the mechanistically relevant ferrous active site of BLM, is consistent with two possible models of the first coordination sphere for resting Fe^{II}BLM. The pyrimidine, imidazole, deprotonated amide, and secondary and primary amine ligands are bound in a pseudo-square-pyramidal geometry with either the 3-*O*-carbamoyl substituent of the mannose sugar or solvent occupying the sixth site trans to the primary amine. Direct coordination of the carbamoyl group would necessitate chirality at the Fe center opposite to that observed for HOO-Co^{III}BLM.[43] In the proposed Co chirality, the primary amine and sugar moiety are confined to the same face of the equatorial plane with only the primary amine bound to the metal trans to the exogenous hydroperoxide ligand. If the HOO-CoBLM complex is an appropriate model for activated FeBLM as is supported by a recent NMR study[61] on the Fe^{II}BLM complex, this would suggest that the effect of carbamoyl variability associated with the CD and MCD spectral changes at the Fe^{II} active site of BLM occurs in the second coordination sphere of the metal. Such a perturbation could result from steric interactions between the carbamoyl substituent and an active site ligand such as the primary amine, perhaps through H-bonding. Eliminating these steric constraints in the *iso* or decarbamoyl derivatives might weaken the Fe-primary amine bond and account for the decrease in ligand field strength at the site. It may be noted, however, that in another NMR study of a HOO-Co^{III}BLM derivative, the carbamoyl group has been proposed to be an axial ligand.[97]

With a six-coordinate Fe^{II} active site in the resting form of the drug, dioxygen known to bind prior to formation of activated BLM, and a seven-coordinate intermediate structure improbable, a dissociative mechanism requiring release of a ligand seems mechanistically most plausible. The room-temperature CD spectra for Fe^{II}BLM/PEPLM, $Fe^{II}iso$-PEPLM, and Fe^{II}DP-PEPLM are all quite different from one another and consistent with the two possible interpretations of the MCD spectral data presented above. Upon binding of azide (a small molecule probe of the dioxygen binding site), the Fe^{II}BLM/PEPLM and $Fe^{II}iso$-PEPLM spectra change to an identical form whereas the Fe^{II}DP-PEPLM spectrum is quite different. This is consistent with the assignment of the sixth ligand as the carbamoyl substituent as illustrated in the following scheme.

BLM (PEPLM)   iso-**PEPLM**
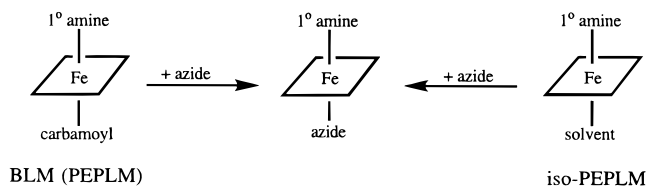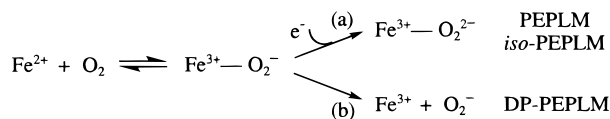
Alternatively, it is possible that replacing a solvent molecule at the sixth site by the exogenous anion would reduce the second coordination sphere differences between the resting and carbamoyl modified derivatives. In either case, there is no difference in the observed spectral features of the small-molecule-bound active sites of Fe^{II}BLM/PEPLM and $Fe^{II}iso$-PEPLM. Scatchard analysis gives an azide binding constant of ~60 M^{-1} for Fe^{II}BLM/PEPLM which is twice as great as the 25 M^{-1} binding constant observed for $Fe^{II}iso$-PEPLM. As the azide-bound forms are structurally equivalent this difference in binding affinities must be attributed to an increased stability of the exchangeable ligand in *iso*-PEPLM vs BLM/PEPLM. This correlates with the decreased DNA cleavage efficiency reported for this class of derivatives relative to the unmodified drug. For Fe^{II}DP-PEPLM, the exact position of azide binding is not determined, although the resulting ligand set and structure at the ferrous site is clearly different than observed for the azide-bound forms of both BLM/PEPLM and *iso*-PEPLM (see Figure 4).

In addition to the geometrical information obtained through the excited-state ligand field CD and MCD analyses, the electronic structures of the ferrous forms of these derivatives have been elucidated through ground-state ligand field and excited-state charge transfer MCD studies. The unusually low value of δ and the low-energy MLCT transitions observed for resting Fe^{II}BLM[52] are unaffected by altering the terminal amine moiety attached to the bithiazole, suggesting that the electronic nature of the Fe d-orbital manifold and relative energies of the pyrimidine π^*-orbitals are insensitive to this distant ligand framework perturbation. The value of δ observed in $Fe^{II}iso$-PEPLM increases (from 2.4 to 4.8 cm^{-1}) but there is no change in the energies of the MLCT envelopes. Thus the total splitting of the d$_\pi$-orbitals decreases ($\Delta^5T_{2g} \sim$ 790 cm^{-1} vs 1040 cm^{-1} for Fe^{II}PEPLM) in the derivatives with perturbations to the sugar moiety, but there is little direct effect on the Fe-pyrimidine π-bonding interactions as evidenced by the unaltered MLCT transition energies. In Fe^{II}DP-PEPLM, the value of δ is also increased (to 4.4 cm^{-1}) with a similar total splitting of the d$_\pi$-orbitals to ~800 cm^{-1}, which is still somewhat larger than observed for non-heme iron systems with innocent ligands, reflecting the presence of the pyrimidine moiety. However, it is important to realize that the large increase in the ^5E_g splitting observed for DP-PEPLM would suggest a parallel increase in the $^5T_{2g}$ splitting, when in fact this splitting decreases and indicates reduced π-interactions with the ligand. This correlates with the shift to higher energy of the MLCT transitions and indicates a diminished degree of Fe^{II}→pyrimidine back-bonding. Substitution of the primary amine ligand with a solvent molecule therefore has a pronounced effect on the electronic structure and π-interactions specifically with the pyrimidine ligand at the Fe^{II} site. Replacing the stronger field primary amine, a σ-donor, by the weaker field solvent molecule, a σ-donor/π-donor, lowers the energy of the Fe d-manifold relative to the pyrimidine π^*-acceptor orbitals and increases the energies of the d$_\pi$→π^* MLCT transitions in the perturbed species. The presence of the electron donating primary amine in unmodified BLM places relatively more negative character at the metal center and allows for facile back-bonding to the pyrimidine.

This back-bonding is directly related to the oxygen reactivity at the Fe^{II} site. For resting Fe^{II}BLM, back-bonding to the pyrimidine ligand decreases the extent of charge transfer to the bound oxygen molecule making FeBLM less likely to dissociate superoxide and more susceptible to further reduction to form the peroxide-level activated BLM intermediate en route to DNA strand scission as shown in pathway (a) in the following scheme.[52] In contrast, most non-heme iron systems which lack π-acceptor interactions with a ligand autoxidize in the presence of oxygen to form high-spin Fe^{III} and superoxide radicals

following pathway (b) below.[98]

$$Fe^{2+} + O_2 \rightleftharpoons Fe^{3+}—O_2^- \begin{array}{c} \xrightarrow{\quad e^- \quad (a)} Fe^{3+}—O_2^{2-} \quad \begin{array}{l} PEPLM \\ \textit{iso}\text{-PEPLM} \end{array} \\ \xrightarrow{\qquad (b)} Fe^{3+} + O_2^- \quad DP\text{-PEPLM} \end{array}$$

For the derivatives in which the Fe−pyrimidine interactions are unchanged by the ligand perturbation, DNA cleavage still occurs with a modest level of efficiency and similar specificity, indicating that the mechanism of oxygen activation at the active site is not significantly affected by the modification; i.e., Fe^{II}-PEPLM- and Fe^{II}*iso*-PEPLM-containing classes of derivatives react with dioxygen via pathway (a). For the derivatives in which the Fe−pyrimidine interactions are greatly reduced (increased δ and higher energy MLCT bands) there is no DNA cleavage observed and a high-spin ferric complex is produced upon reaction with dioxygen; i.e., Fe^{II}DP-PEPLM in which the primary amine of the β-aminoalanine has been eliminated reacts with dioxygen via pathway (b). Thus, perturbing the axial primary amine significantly affects the degree of Fe→pyrimidine back-bonding; this electronic stabilization is a necessary requirement for the proper functioning of the drug−dioxygen complex in forming activated BLM.

In summary, our studies have provided significant insight into the structure and reactivity of Fe^{II}BLM. The resting site is six-coordinate with a coordination sphere of at least five endogenous ligands, including the primary amine of the β-aminoalanine amide fragment as well as either the 3-*O*-carbamoyl substituent of the mannose sugar or solvent bound trans to this axial position. The sixth site occupied by this weakly bound ligand is the exchangeable site of exogenous ligand binding. The 3-*O*-carbamoyl substituent of the mannose sugar is either directly coordinated to the metal in one orientation of the ligands about the Fe or sterically interacts with an active site ligand, perhaps through H-bonding in the opposite chirality. Perturbing the carbamoyl moiety diminishes the extent of small molecule reactivity and DNA cleavage. Additionally, removing the axial primary amine reduces the Fe−pyrimidine π-back-bonding interactions and significantly affects the observed oxygen chemistry. Sufficient π-back-bonding is required to electronically stabilize the initial Fe^{III}−O$_2^-$ intermediate from loss of superoxide or reaction with substrate and allow the formation of activated BLM, the last observed intermediate kinetically competent to cleave DNA.

Supporting Information Available: Three figures and accompanying text illustrating the similarity of the MCD spectral features within each of three classes of BLM derivatives with perturbations to the terminal amine moiety of the bithiazole (Fe^{II}-BLM, Fe^{II}BLM A$_2$, Fe^{II}BLM B$_2$, Fe^{II}BLM demethyl A$_2$, and Fe^{II}PEPLM), the carbamoyl substituent of the mannose sugar (Fe^{II}*iso*-PEPLM, Fe^{II}*iso*-BLM A$_2$, and Fe^{II}decarbamoyl-BLM A$_2$), and the primary amine of the β-aminoalanine fragment (Fe^{II}-DP-PEPLM and Fe^{II}*N*-acetyl BLM A$_2$) (6 pages). See any current masthead page for ordering and Internet access instructions.

JA971839Q

(97) Caceres-Cortes, J.; Sugiyama, H.; Ikudome, K.; Saito, I.; Wang, A. H.-J. *Eur. J. Biochem.* **1997**, *244*, 818−828.

(98) Feig, A. L.; Lippard, S. J. *Chem. Rev. (Washington, D.C.)* **1994**, *94*, 759−805.